The Nature of Elliptical Galaxies, Proceedings of the Second Stromlo Symposium, Eds. M. Arnaboldi, G.S. Da Costa & P. Saha

Gravitational Lensing Limits On Early-Type Galaxies

C.S. Kochanek & C.R. Keeton

Harvard-Smithsonian Center for Astrophysics

Abstract: Gravitational lenses are a unique new constraint on the structure of galaxies. We review the evidence that most lenses are early-type galaxies, the optical properties of the lens galaxies, the evidence against constant M/L models, recent work on the axis ratios of the mass distribution, and the role stellar dynamics plays in gravitational lensing.

1. Introduction

Gravitational lenses directly determine the transverse gravitational accelerations in a distant galaxy or cluster. Thus, they share the advantages of X-ray emission over stellar dynamics by avoiding all the additional assumptions needed to interpret line-of-sight velocities, and they can measure some properties of the lens galaxy with unprecedented accuracy. Nothing, however, is a panacea. In particular, lenses are sensitive to gravitational perturbations along the line-of-sight between the observer and the source. Rarity cannot be considered a major weakness of gravitational lenses any longer, since the number of galaxy-dominated lenses is ~ 25 and continuing to increase. In our brief review we will emphasize physical results relating to the structure of galaxies, and we will review neither the physics of gravitational lensing (see Narayan & Bartelmann (1996) or Schneider, Ehlers & Falco (1992)) nor the details of the observational data (see Keeton & Kochanek 1996a).

Gravitational lenses constrain the properties of galaxies through their statistical properties (numbers, image separations, morphologies etc.), detailed models of individual lenses, and comparisons of the lens models to the optical properties of the lens galaxies and stellar dynamical models. The issues we will discuss are (1) why we believe most of the lenses are early-type galaxies; (2) the mass scale (or mass-to-light ratio) and the radial mass distribution of the lens galaxies; (3) the axis ratios of early-type galaxies; and (4) the interplay between gravitational lensing and stellar dynamics.

2. Lens Galaxy Colors and Luminosities

The mean image separation in a gravitational lens sample depends largely on the typical velocity dispersion, $\Delta\theta \propto (\sigma/c)^2$, unless the numbers or properties of the lenses evolve rapidly at redshifts less than unity. The numbers of lenses found in surveys depends on the cosmological model through the comoving volume to the source D^3, the comoving density of lenses n_*, and the square of the mean separation (the cross section), $N \propto n_* \Delta\theta_*^2 D^3$ (e.g. Turner, Ostriker &

Gott 1984, Maoz & Rix 1993, Kochanek 1996). The $*$ denotes the values for a typical L_* galaxy. Hence we can estimate the relative numbers of spiral and early-type lens galaxies by the ratios of the products $n_*\sigma_*^4$. While the spirals are more numerous ($n_e/n_s \sim 0.75 \pm 0.36$, Marzke et al. 1994), the early-types are significantly more massive ($\sigma_e/\sigma_s \sim 1.5 \pm 0.15$), so we expect most lenses will be early-types in the ratio of about 4 ± 2. Spiral lenses have larger amounts of extinction and smaller average image separations than early-type lenses, reducing their detectability in optical and low resolution surveys respectively.

The optical data on lens galaxies are poor and inhomogeneous. Ground based and WF/PC 1 images are limited by problems with resolution and contrast relative to the images. Moreover, many published lens magnitudes do not include the definition of the aperture used to determine the magnitude, and a remarkably heterogeneous set of filters was used for the observations. We hope to obtain a complete set of V, I, and H images of all known lens galaxies in Cycle 7 to put the optical data on a firmer footing, but in Keeton et al. (1996) we attempt to systematically review the existing optical data.

Figure 1 shows the colors of the lens galaxies compared to standard Bruzual & Charlot (1993) evolution models. It is difficult to condense the results into a simple figure because no filter pair was used for more than two lens galaxies. The lens galaxies are generally as red or somewhat redder than expected for early-type galaxies. One lens, MG 0414+0534, is far redder than the models, and one lens, B 0218+357, is bluer. B 0218+357 also shows HI absorption (Carilli et al. 1993), making it the best candidate for a spiral lens in Figure 1.

In Figure 2 we compare the ($z = 0$) absolute B magnitude of the lenses (using the evolution models to estimate the magnitude) to the cosmology-corrected image separation (for $\Omega_0 = 1$), to produce the lensing equivalent of the Tully-Fisher or Faber-Jackson relation. The problems with the lens magnitudes are more severe here, and the typical uncertainties are probably 0.5 mag. Nonetheless, there is broad agreement between the observed and expected luminosities. We treated B 0218+357 as a spiral, and it would lie near MG 0751+2716 if treated as an elliptical. MG 0414+0534 again lies far off the locus of all other lens galaxies. Its very red spectrum is extremely peculiar, because most dusty galaxies also have strong blue emission from ongoing star formation.

3. The Mass Scale and Radial Mass Density

Unlike the luminosity of the lens galaxy, the mass inside the "ring" defined by the lensed images is usually known to $\sim$1% for the four-image systems and radio rings and to $\sim$10% for the two-image systems. The absolute scale depends on the Hubble constant, weakly on the cosmological model (usually 5–10%), and weakly on potential perturbations along the line of sight (also 5–10% at worst). Such accuracy for a mass determination is unmatched by any other probe of galactic structure except spiral galaxy rotation curves.

Maoz & Rix (1993) established that de Vaucouleurs models with the van der Marel (1991) mass normalization of $(M/L)_{B*} = (10 \pm 2)h$ are unable to

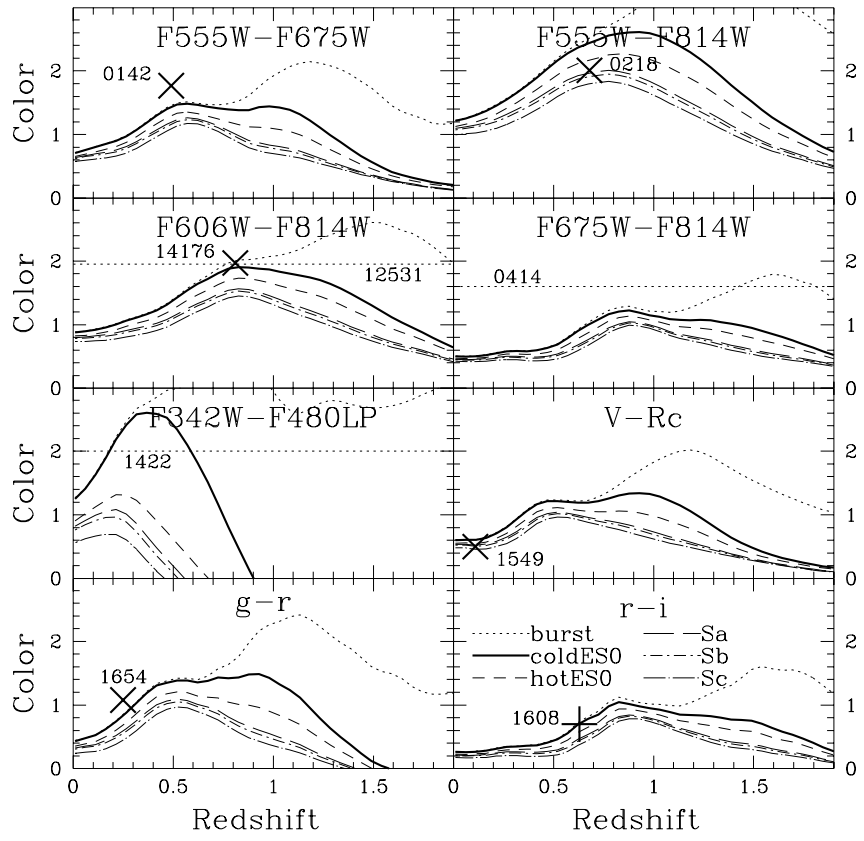

Figure 1. Lens galaxy colors. The crosses (known lens redshifts) and horizontal dashed lines (unknown lens redshifts) display the lens properties, and the curves are typical early-type to spiral color evolution models. Typical uncertainties are 0.1 to 0.3 mag.

produce the observed image separations, and Kochanek (1996) demonstrated that $(M/L)_{B*} = (20 \pm 4)h$ was required. Most models of individual lens galaxies also have projected mass-to-light ratios inside the "ring" defined by the images of roughly $20h$ (also see Burke et al. 1992), although the scatter and uncertainties are large because of the optical photometry. Figure 3 shows rough estimates of (M/L) as a function of lens redshift. *All the uncertainty in Figure 3 is due to the light rather than the mass!* For example the PG 1115+080 point is a central (undefined) aperture magnitude rather than an integrated magnitude. Given improvements in the optical photometry it is a simple matter to explore the evolution of the mass-to-light ratio with lens redshift. For comparison, if we assume a singular isothermal sphere is the prototypical dark matter model, the dark matter velocity dispersions required to fit the observed lens separations and the stellar dynamics of nearby galaxies agree with $\sigma_* \simeq 225 \pm 20$ km s^{-1} (Kochanek 1994, 1996), and there is no evidence for the $(3/2)^{1/2}$ correction factor introduced by Turner, Ostriker & Gott (1984) (see §5).

Directly determining the radial mass distribution is significantly harder than

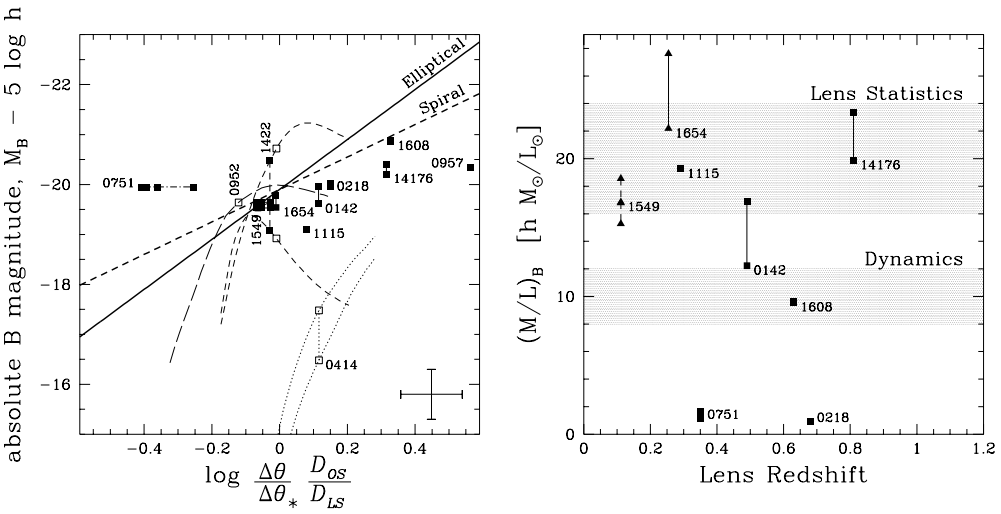

Figure 2. Lens galaxy "Faber-Jackson" relation (left). The estimated zero redshift absolute B magnitude of the lens galaxies as a function of the cosmology-corrected image separations. The predicted correlations for standard models of early-type (solid) and spiral (dashed) galaxies are shown by the heavy lines. The filled points mark lenses with known lens redshifts, connected by a vertical line if we have estimates using more than one color. Filled points connected by a horizontal line (MG 0751+2716) show the effects of not knowing the source redshift. Empty points mark the values for the most probable lens redshift where it is unknown, and the curves cover the range of probable lens redshifts. The large error bar shows the level at which the curves and points can be shifted relative to each other because of uncertainties in M_{B*} and $\Delta\theta_*$.
Figure 3. Estimated B mass-to-light ratios of lens galaxies corrected to $z = 0$ (right). The scatter is the same as in Figure 2, but the switch to a linear scale highlights the problems with the optical magnitudes. For lenses marked by triangles we have reasonable estimates of the aperture corrections, while for the squares we do not. Note that the probable spiral lens B 0218+357 has a significantly lower M/L.

determining the enclosed mass. Kochanek (1991, also Wambsganss & Paczyński 1994) demonstrated that most lens geometries are insensitive to the radial mass distribution because all the images lie at a common radius from the center of the lens galaxy. Only systems with images at significantly different radii, or equivalently with extended radio emission, can directly attack the issue of the radial mass distribution. The two published cases are the MG 1654+134 radio ring (Kochanek 1995) and the 0957+561 VLBI double (Grogin & Narayan 1996), both of which are most consistent with singular isothermal mass distributions. We generally find that many lenses weakly favor flat rotation curves and slowly declining surface densities over more centrally concentrated models.

4. Ellipticities and External Perturbations

Most lens geometries accurately measure an ellipticity and an orientation for the lens galaxy. The orientation is strongly constrained (to $\sim 1^\circ$ in a four-image lens) and independent of the monopole structure of the lens, while the required shear depends on the monopole structure. The required ellipticity or shear scales as $(1 - \kappa_r)$ where κ_r is the surface mass density of the monopole at the radius of the ring in units of the critical surface mass density for lensing (Kochanek 1991). Centrally concentrated models ($\kappa_r \simeq 0$) require twice as much

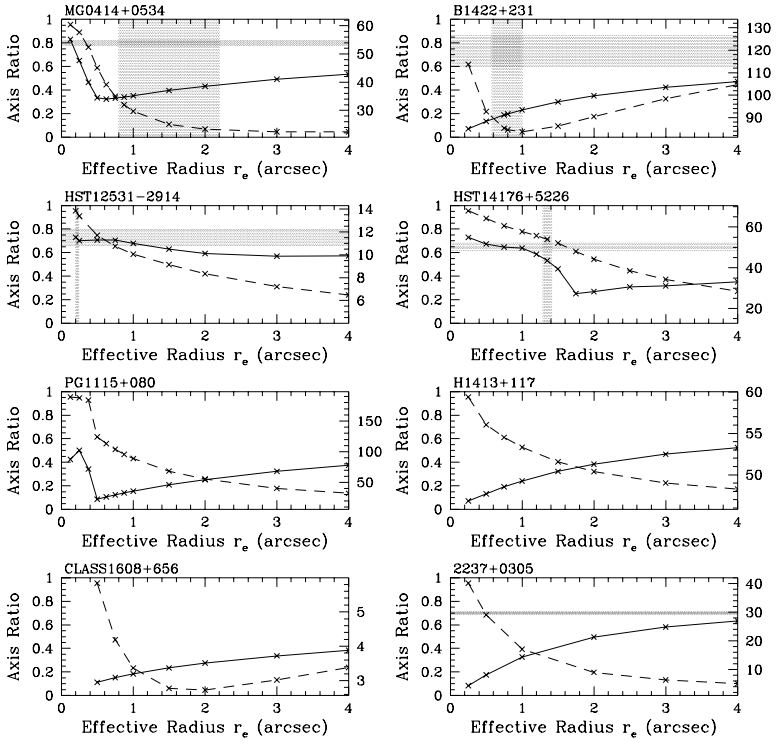

Figure 4. χ^2/N_{dof} goodness-of-fit (right scale, dashed lines) and model axis ratios (left scale, solid lines) for fitting the observed lenses with an ellipsoidal de Vaucouleurs model. The grey bands mark the observational limits on the effective radius and axis ratio when known.

ellipticity as isothermal models ($\kappa_r \simeq 1/2$). The axis ratio differences between the centrally concentrated, modified-Hubble models used by Nair (1996) and isothermal models are due to this scaling.

We have undertaken a survey to fit all the available lenses using ellipsoidal de Vaucouleurs and softened power-law density profiles ranging from isothermal through modified-Hubble and Plummer models (Keeton & Kochanek 1996b). For example, Figure 4 shows the χ^2 and axis ratios for ellipsoidal de Vaucouleurs models of eight lenses as a function of the effective radius. The model both fails to fit the data and requires an unusually flattened galaxy for most of the lenses. If we switch to a singular isothermal ellipsoid, the required lens galaxy ellipticities decrease and the χ^2 of the fits improve. Figure 5 shows the best-fit axis ratios for a sample of four-image, radio ring, and two-image lenses. As expected from theory, the four-image lenses are flatter than the radio rings which are flatter than the two image lenses.

The relative numbers of different image morphologies also constrain the axis ratio because the cross sections are functions of the ellipticity. For example, the four-image cross section is proportional to ϵ^2. Figure 6 shows the expected number of two-image, four-image, and three-image cusp lenses as a

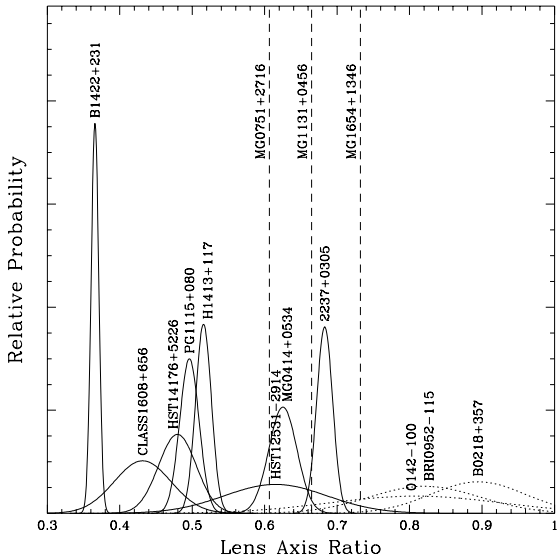

Figure 5. Model axis ratios for singular isothermal ellipsoids with four images (solid), radio rings (vertical dashed lines), and two images (dotted). We expect the clear ordering of the axis ratios with morphology from the cross sections. These axis ratio estimates may be contaminated by external tidal perturbations. The axis ratios increase if we use more centrally concentrated ellipsoids.

function of the axis ratio of a singular isothermal ellipsoid. The three-image cusp configuration has three co-linear images offset to one side of the lens center and has yet to be observed. The observed sample has roughly equal numbers of two-image and four-image systems, which requires lenses with a mean axis ratio of nearly 2:1. Ellipsoids are much more efficient at producing four-image lenses than external tidal perturbations, and as first noted by King & Browne (1996) the typical external shear perturbation γ required to fit the individual lenses woefully underpredicts the observed number of four-image lenses. Witt (1996) has also shown that some lens galaxy positions are inconsistent with external shear as the sole angular perturbation. The observed axis ratio distribution for early-type galaxies, *including both true ellipticals and the flatter S0s*, is statistically consistent with the distribution needed to produce the observed numbers of four-image lenses and to fit the individual lenses using singular isothermal ellipsoids. One problem we have yet to treat properly is the relative normalization of models with differing axis ratios (see §5) – for a fixed amount of mass, flattened models generally produce more lenses than spherical models.

No lens we have examined, however, is well fit by a single ellipsoidal density, but all lenses are well fit by the combination of an ellipsoid and an independent external shear (Keeton, Kochanek & Seljak 1996). The dramatic improvement in the goodness of fit with the addition of a second shear axis is a marked contrast to changes in the radial density distribution, where most lenses are equally well (or poorly) fit by radically differing radial profiles (Kochanek 1991, Wambsganss & Paczyński 1994). The origin of the second shear axis has yet

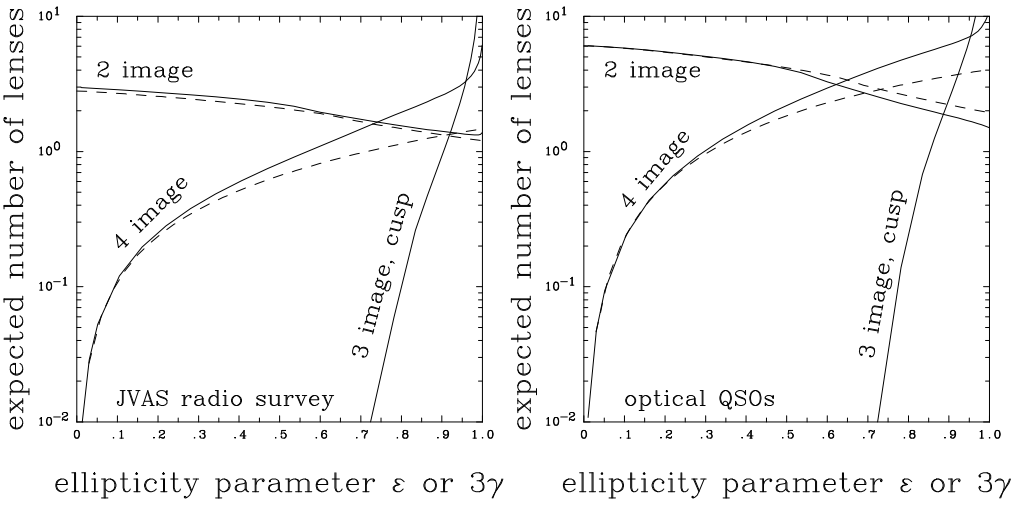

Figure 6. Expected numbers of two-image, four-image and three-image cusp lenses as a function of the external shear γ (dashed) or eccentricity ϵ (solid) for the JVAS radio lens survey (left, see King & Browne 1996) and optical QSO lens surveys (right). The lens axis ratio is $r = (1-\epsilon)^{1/2}/(1+\epsilon)^{1/2} \simeq 1-\epsilon$ for singular isothermal ellipsoids.

to be fully understood, since there are three possible sources. First, if the dark matter halo and the galaxy are aligned but have differing triaxialities, then the projected dark matter can be misaligned from the projected light (like the kinematic misalignment angle, e.g. Franx et al. 1991). Second, the dark matter and the stars may not be in equilibrium, so that they are intrinsically misaligned. Third, there are external (tidal) perturbations due to (in descending order of importance) galaxies, groups, and clusters correlated with the primary lens galaxy or near the line of sight (Kochanek & Apostolakis 1988), and weaker perturbations due to large scale structure (Bar-Kana 1996). Several lenses (e.g. B 1422+231 (Hogg & Blandford 1994) and PG 1115+080 (Schechter et al. 1996)) appear to be part of a small group of galaxies, where the other galaxies have the correct positions to account for the secondary shear. Surprisingly, we find that the external shear perturbations have very little effect on the expected numbers of lenses even when they are large enough to significantly alter the fits to the individual lenses.

The relative orientations of the major axes of the model and the stellar distribution are a clean geometric test for the existence of both external (tidal) perturbations and misalignments between the dark matter and the stars. Unfortunately the available data are sparse and ambiguous. In B 1422+231 the model and observed galaxy are aligned to $6^\circ \pm 15^\circ$ even though it is one of the strongest cases for the presence of large external tidal perturbations (see Hogg & Blandford 1994), in MG 0414+0534 they are aligned to $8^\circ \pm 5^\circ$, in HST 12531–2914 they are aligned to $3^\circ \pm 3^\circ$, and in HST 14176+5226 they are aligned to $11^\circ \pm 2^\circ$. Larger samples and reduced uncertainties in the galaxy orientations are needed to determine the alignment distribution. Whatever the source of the second axis, the misalignments will be larger for two-image lenses than four-image lenses. Unfortunately, the lens model alignments are less certain for the two-image systems unless the lens galaxy position and image flux ratios are well

constrained.

5. What Can Stellar Dynamics Do For Lensing?

Stellar dynamical models are important for normalization problems in gravitational lensing. For example, if we want to avoid using the observed image separations to normalize the masses of galaxies, we must use existing stellar dynamical estimates. When doing so, it is important to use self-consistent models and to avoid oversimplifications. As we mentioned in §3, an oversimplified stellar dynamical model introduced by Turner, Ostriker & Gott (1984) implied that the dark matter dispersion σ_{dm} for isothermal lens models should be $\sigma_{dm} = (3/2)^{1/2}\sigma_c$ larger than the central velocity dispersion of the stars σ_c. Kochanek (1994) demonstrated that using the true luminosity profiles of galaxies (rather than an r^{-3} power law) and the typical aperture sizes used in the dispersion measurements (rather than averaging over the entire galaxy) leads to $\sigma_{dm} \simeq \sigma_c$. Since the image separations scale as σ_{dm}^2 and the number of lenses scale as σ_{dm}^4, the use of the poor dynamical model caused an overestimate of the image separations by 50%, and of the number of lenses by 125%. The resulting difference in the estimated cosmological matter density is $\Delta\Omega_0 \simeq 0.5$.

Oversimplifying the dynamical normalization can also bias inferences about other parameters of the mass distribution. For example, if we add a core radius s to a dark matter distribution (e.g. $\rho \propto \sigma_{dm}^2/(r^2+s^2)$) then we must increase the velocity dispersion σ_{dm} to compensate for the reduced mass near the galactic center. The singular model was normalized to fit the observed central velocity distribution of the stars, and if we do not adjust σ_{dm} upwards, the softened models will no longer fit the observations. The correction to σ_{dm} is small (5–10%), but it becomes a 10–20% correction in the separations, and a 20-40% correction in the expected number of lenses! *These systematic corrections are qualitatively and quantitatively important, and models that fail to include them will be wrong.* With the addition of elliptical structure, the normalization problem becomes considerably more difficult, and we have yet to treat the problem in detail. Finally, in 0957+561 (e.g. Rhee 1991, Falco et al. 1996) there are measurements of the central velocity dispersion of the lens galaxy, which are used to estimate the Hubble constant from the lensing time delay. We must use dynamical models combining the mass profiles inferred from lensing with the luminosity profile of the galaxy to interpret the results (e.g. Grogin & Narayan 1996). Failure to include the full range of dynamical uncertainties (e.g. orbital isotropy) in the models will lead to underestimates of the uncertainties in the Hubble constant.

6. Summary

The optical properties of the lens galaxies are generally consistent with most lenses being early-type galaxies with standard luminosities and colors. There are exceptions such as MG 0414+0534, which is both anomalously red and faint, and B 0218+357, which is bluer, brighter and contains HI gas (i.e. a spiral). The heterogeneity of the data and imprecise aperture definitions make it difficult

to compare lens galaxies to normal galaxies, but the results semi-quantitatively agree with standard models. We desperately need to observe the lens galaxies using a uniform set of filters and to carefully estimate their magnitudes, colors, axis ratios, and orientations. We could then, for example, track the evolution of mass-to-light ratios with redshift.

Constant M/L models appear to be are inconsistent with the lens data. The value of M/L needed to fit the image separations is double the stellar dynamical estimate, and ellipsoidal de Vaucouleurs models of individual lenses usually have large χ^2 statistics and large ellipticities. Models with flat rotation curves normalized to fit the image separations are consistent with stellar dynamics, are better lens models and have lower axis ratios. Progress in determining the radial mass profile using lensing depends on models of lenses with radial structure to the images. Most of these lenses are radio rings, and we need deeper maps with better visibility coverage to take full advantage of the rings as tools for probing the lens galaxies.

We have yet to understand the effects of external tidal perturbations on the lens models. External perturbations are certainly present in several lenses (e.g. B 1422+231 and PG 1115+080), but their amplitudes are hard to calibrate because many effects of tidal perturbations can be mimicked by dark matter halos. After all, if the radial mass distribution is dominated by dark matter we should not be surprised if the angular mass distribution has a different axis ratio or triaxiality than the luminous matter. Galaxy formation simulations usually produce halos that are both flatter and more triaxial than the visible stars (e.g. Warren et al. 1992, Dubinski 1992, 1994). The distribution of misalignment angles between the major axes of the lens models and the visible lens galaxies should be a good geometric probe of these problems.

The extreme sensitivity of lensing results to the mass scale of the galaxies means that it is usually safer to determine the mass scale using the observed image separations rather than stellar dynamical models. If stellar dynamical models are used to set the masses, it is absolutely critical to use self-consistent models. Franx (see these proceedings) has convincingly demonstrated that it is possible to measure velocity dispersions in galaxies comparable to the typical lens galaxy. We should try to determine the central velocity dispersions of the brighter lens galaxies to test and compare the lensing and stellar dynamical models.

Acknowledgements: We thank E. Falco, J. Hewitt, R. Narayan and P. Schechter for collaborations and discussions. CSK is supported by NSF grant AST-9401722, and CRK is supported by a National Defense, Science & Engineering Fellowship.

References

Bar-Kana, R., 1996, ApJ, 468, 17

Bruzual, G.A., & Charlot, S., 1993, ApJ, 405, 538

Burke, B.F., Lehàr, J., & Conner, S.R., 1992, in Gravitational Lenses, eds., Kayser, R., Schramm, T., & Nieser, L., (Springer: Berlin) 237

Carilli, C.L., Rupen, M.P., & Yanny, B., 1993, ApJ, 412, 59

Dubinski, J., 1992, ApJ, 401, 441

Dubinski, J., 1994, ApJ, 431, 617

Falco, E.E., Shapiro, I.I., Moustakas, L.A., & Davis, M., 1996, astro-ph

Franx, M., Illingworth, G., & De Zeeuw, T., 1991, ApJ 383, 112

Grogin, N., & Narayan, R., 1996, ApJ, 464, 92

Hogg, D.W., & Blandford, R.D., 1994, MNRAS, 268, 889

King, L.J. & Browne, I.W.A., 1996, MNRAS, 282, 67

Keeton, C.R., & Kochanek, C.S., 1996a, in Astrophysical Applications of Gravitational Lensing, IAU 173, eds., C.S. Kochanek & J.N. Hewitt (Dordrecht: Kluwer) 419

Keeton, C.R., Kochanek, C.S., & Seljak, U., 1996, astro-ph/9610163

Keeton, C.R., Kochanek, C.S., & Falco, E.E., 1996, in preparation

Keeton, C.R., & Kochanek, C.S., 1996b, in preparation

Kochanek, C.S., & Apostolakis, J., 1988, MNRAS, 235, 1073

Kochanek, C.S., 1991, ApJ, 373, 354

Kochanek, C.S., 1994, ApJ, 436, 56

Kochanek, C.S., 1995, ApJ, 445, 559

Kochanek, C.S., 1996, ApJ, 466, 638

Maoz, D., & Rix, H.-W., 1993, ApJ, 416, 425

Marzke, R.O., Geller, M.J., Huchra, J.P., & Corwin, H.G., 1994, AJ, 108, 437

Nair, S., 1996, in Astrophysical Applications of Gravitational Lensing, IAU 173, eds., C.S. Kochanek & J.N. Hewitt (Dordrecht: Kluwer) 197

Narayan, R., & Bartelmann, M., 1996, in the 1995 Jerusalem Winter School

Rhee, G., 1991, Nature, 350, 211

Schechter, P.L., Bailyn, C.D., Barr, R., et al., 1996, astro-ph/9611051

Schneider, P., Ehlers, J., & Falco, E.E., 1992, Gravitational Lenses, (Berlin: Springer)

Turner, E., Ostriker, J.P, & Gott, J.R., 1984, ApJ, 284, 1

van der Marel, R.P., 1991, MNRAS, 253, 710

Wambsganss, J., & Paczyński, B., 1994, AJ, 108, 1156

Warren, M.S., Quinn, P.J., Salmon, J.K., & Zurek, W.H., 1992, ApJ, 399, 405

Witt, H.J., 1996, astro-ph/9608197